Rotor Design of a High-Speed Permanent Magnet Synchronous Machine rating 100,000 rpm at 10 kW

Björn Riemer, Marc Leßmann, Kay Hameyer
Institute of Electrical Machines - RWTH Aachen University
Schinkelstraße 4, D-52056 Aachen, Germany
phone: (+49)-241-80-97667, fax: (+49)-241-80-92270
Email: Bjoern.Riemer@iem.rwth-aachen.de

***Abstract*—Rotors of electrical high speed machines are subject to high stress, limiting the rated power of the machines. This paper describes the design process of a high-speed rotor of a Permanent Magnet Synchronous Machine (PMSM) for a rated power of 10 kW at 100,000 rpm. Therefore, at the initial design the impact of the rotor radius to critical parameters is analyzed analytically. In particular, critical parameters are mechanical stress due to high centrifugal forces and natural bending frequencies. Furthermore, air friction losses, heating the rotor and the stator additionally, are no longer negligible compared to conventional machines and must be considered in the design process. These mechanical attributes are controversial to the electromagnetic design, increasing the effective magnetic air gap, for example. Thus, investigations are performed to achieve sufficient mechanical strength without a significant reduction of air gap flux density or causing thermal problems. After initial design by means of analytical estimations, an optimization of rotor geometry and materials is performed by means of the finite element method (FEM).**

***Index Terms*—High-speed PMSM, yield strength, rotor dynamics, natural bending frequency, air friction losses.**

I. Introduction

The actual change of electricity supply networks toward a local structure with an advanced integration of renewable energies boosts the application of micro gas turbines, consuming each kind of gaseous or liquid biofuel. Micro gas turbines operate at speeds up to 200,000 rpm, requiring a lossy two-shaft turbine concept or a wear prone transmission gear if coupled with conventional generators. These disadvantageous components can be omitted by a direct coupling of the generator shaft with the turbine. Due to the linear dependency between rotor volume and motor torque, the power density of the generator can be increased for several orders of magnitude compared with high torque machines. Limiting factors for achievable power are the mechanical rotor properties such as strength and natural frequencies. The maximum radius of a high-speed machine rotor is limited by stress induced by centrifugal forces. Its length is delimited by the natural bending frequencies. Furthermore, friction losses are not negligible in high-speed applications compared to classical machines, increasing the rotor and stator temperature additionally. On the one hand an impermissible rise of rotor temperature reduces the mechanical strength of the rotor materials, on the other hand the permanent magnetic material might be demagnetized. Additionally, the application of classical bearings in high-speed machines is limited due to the high circumferential speed of the shaft. Thus, by the application of magnetic bearings higher speeds can be achieved. Due to the reduced force density of magnetic bearings compared to classical bearings, an air gap winding in the stator for minimization of the attraction forces at radial rotor displacement is advantageous. Thus, axial construction space for the bearing can be replaced by additional rotor volume, increasing the achievable torque of the motor.

This paper describes design criteria of the rotor of a high-speed permanent magnet synchronous machine (PMSM), using the example of a motor with a rated power of 10 kW at 100,000 rpm. Starting with a determination of the required rotor volume, in the second design step the mechanical stress induced by centrifugal forces is investigated. Different approaches of permanent magnet fixation to the rotor are analyzed, followed by the determination of natural frequencies. Air friction losses are computed in the air gap and at the end face of the rotor to determine the rise of rotor temperature. With respect to the mechanical properties, the electromagnetic design of the rotor is performed. To maximize the power density of the motor, investigations are performed to achieve sufficient mechanical strength without a significant reduction of air gap flux density. Hence, calculations with a ferromagnetic rotor material are compared with a non-magnetic titanium alloy.

II. Initial design

The tangential force, acting on the outer rotor radius of an electrical machine, can be determined by evaluating the Maxwell stress tensor by [2]:

$$F_t = \mu \cdot l_i \cdot \int_0^{2\pi r} H_t \cdot H_n dx, \tag{1}$$

with the the magnetic permeability μ, the active rotor length l_i, the rotor radius r and the tangential and normal magnetic field strength in the air gap $H_{t,n}$. The normal component of the magnetic field strength for a permanent magnet excited synchronous machine is given by:

$$H_n(x) = \frac{1}{\mu} \cdot \frac{B_r}{1 + \frac{\delta}{h_{PM}}} \cdot sin\left(\frac{x}{r}\right), \tag{2}$$

with the remanent flux density B_r of the permanent magnetic material, the height of the permanent magnets h_{PM} and the air

TABLE I
REQUIRED ROTOR VOLUME FOR RATED TORQUE.

	Unit	Value
P_n	[W]	10,000
M_n	$[Nm]$	0.95
n_n	$[1/\mathrm{min}]$	100,000
A_1	$\left[\frac{A}{m}\right]$	10,076
B_r	$[T]$	1.2
δ	$[mm]$	5
h_{PM}	$[mm]$	10
V_R	$[mm^3]$	118,000
V_E	$[mm^3]$	354,000

gap length δ. Under negligence of the magnetic voltage drop inside the stator ($\mu_{stator} \rightarrow \infty$), the tangential field strength is equal to the electric loading:

$$H_t(x) = A(x) = A_1 \cdot sin\left(\frac{x}{r} - \psi\right), \quad (3)$$

$$A_1 = \frac{2 \cdot 3 w_1 I_1}{2\pi r} \cdot \sqrt{2}\xi_1, \quad (4)$$

with the electric loading A, the field weakening angle ψ, the number of turns w_1, the r.m.s value of the current I_1 and the winding factor of the fundamental wave ξ_1. To provide the maximum torque, it is assumed that stator and rotor field are perpendicular to each other, i.e. $\psi = 0$. The torque is calculated by:

$$T_r = F_t \cdot r. \quad (5)$$

Under consideration of the required rated torque:

$$T_r = \frac{P}{2\pi n}, \quad (6)$$

with the rated power P and the rated speed n, the constant rotor volume V_R is determined by Equations 1 - 6:

$$V_R = l_i \cdot \pi r^2 = \frac{T_r}{A_1 \cdot \frac{B_r}{1+\frac{\delta}{h_{PM}}}}. \quad (7)$$

For the exemplary rotor design with rated power of 10 kW at 100,000 rpm, a rotor volume of $V_R = 118,000\,\mathrm{mm}^3$ is derived for the assumed specifications listed in Table I. For the determination of the bending frequencies, the magnetic bearings have to be taken into account additionally. As worst case assumption, the length of one bearing is equal to the length of the active part of the rotor. Thus, the entire rotor length amounts to $V_E = 345,000\,\mathrm{mm}^3$. Based on this fixed volume V_E, for further mechanical design the rotor radius is the residual degree of freedom, rotor length is derived accordingly.

III. STRESS ANALYSIS

The mechanical stress applied to the rotor due to centrifugal forces is evaluated by the von-Mises criterion. In order to observe the fundamental physical behavior of centrifugal forces applied to the rotor, a first analysis is performed on an hollow cylinder, rotating along its rotation axis. The main stresses for this cylinder in cylindrical coordinates are calculated by [1]:

$$\sigma_r(r) = \rho\omega^2 r_o^2 \cdot \frac{3-2\nu}{8(1-\nu)} \cdot \left(1 + \frac{r_i^2}{r_o^2} - \frac{r_i^2}{r^2} - \frac{r^2}{r_o^2}\right), \quad (8)$$

$$\sigma_t(r) = \rho\omega^2 r_o^2 \cdot \frac{3-2\nu}{8(1-\nu)} \cdot \ldots \cdot \left(1 + \frac{r_i^2}{r_o^2} + \frac{r_i^2}{r^2} - \frac{(1+2\nu)\,r^2}{(3-2\nu)\,r_o^2}\right), \quad (9)$$

$$\sigma_z(r) = \rho\omega^2 r_o^2 \cdot \frac{2\nu}{8(1-\nu)} \left(1 + \frac{r_i^2}{r_o^2} - 2\frac{r^2}{r_o^2}\right). \quad (10)$$

Negligent the shear stress, the von-Mises stress is computed as:

$$\sigma_v = \sqrt{\frac{1}{2}\left((\sigma_r - \sigma_t)^2 + (\sigma_t - \sigma_z)^2 + (\sigma_z - \sigma_r)^2\right)}. \quad (11)$$

σ_r, σ_t and σ_z are the main stresses of the hollow cylinder in radial, tangential and axial direction. ν is the Poisson's ratio, $r_{i,o}$ are the inner and outer radius of the cylinder, ρ is the density of the cylinder material and ω the angular frequency. r defines the radial position of stress computation. An irreversible deformation of the rotor will not occur until the von-Mises stress exceeds the yield strength of the rotor material. Figure 1 depicts the von-Mises stress of a rotating cylinder as function of the radial position from the center to the outer radius. The maximum von-Mises stress occurs at the center of a solid and at the inner radius of a hollow cylinder. For the case of the hollow cylinder, the maximum von-Mises stress at the inner radius is always twice as high compared to the same radial position of the solid cylinder. To avoid this hot spot of stress, it is recommended to design a solid rotor without a bore hole. Thus, rotor and shaft have to be manufactured out of one massive cylinder. Generally, the following proportionality can be derived from equation 11:

$$\sigma_{vonMises} \propto r^2. \quad (12)$$

Furthermore, stator iron losses has to be taken into account, reducing the electric loading of the machine due to limitations in stator heat dissipation. Because of the linear dependency between hysteresis losses and the square dependency between eddy current losses and the rotor frequency, [3], especially in high speed applications the iron losses induced by field harmonics has to be reduced. Thus, a sinusoidal air gap field is recommended. Surface mounted diametric magnetized permanent magnet rings provide a sinusoidal air gap field. But, due to the high stress and the low flexural strength of rare earth permanent magnet materials [7], the application to high-speed machines is limited. Figure 2 depicts the maximum von-Mises stress related to different permanent magnet materials depending on the outer rotor radius for a permanent magnet height of $h_{PM} = 5\,\mathrm{mm}$. The von-Mises stress exceeds the maximum flexural strength of the permanent magnet material already at small rotor radius. To avoid this high stresses in the magnetic material, a segmentation of the permanent magnet ring and a fixation of these segments to the rotor is

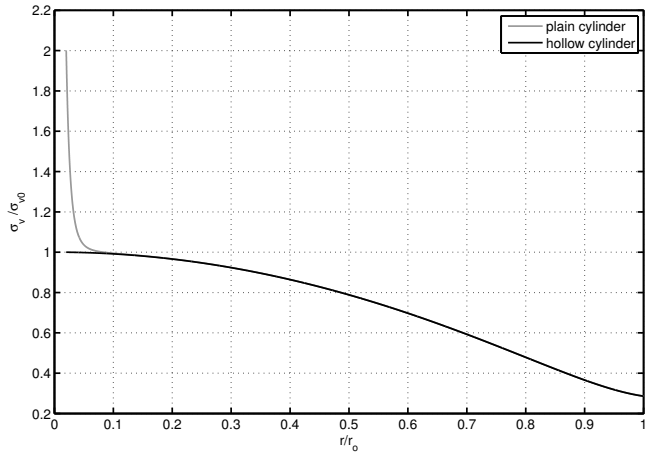

Fig. 1. von Mises stress of a cylinder with bore hole compared with a solid cylinder.

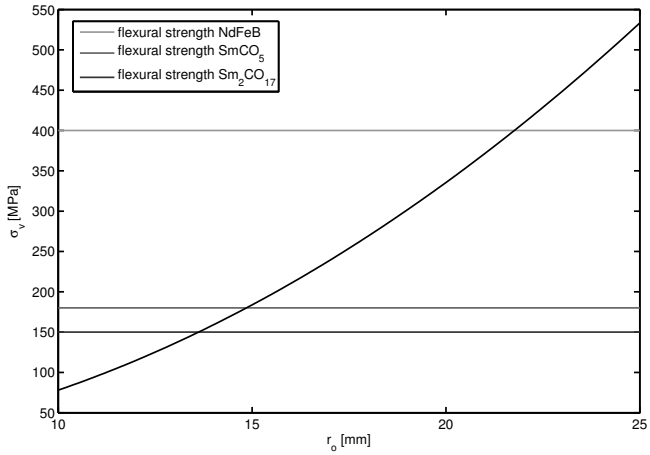

Fig. 2. Maximum von-Mises stress of a permanent magnet ring.

required. A fixation can be performed by a bandage or buried permanent magnets. High tech bandages are made of carbon or glass fiber epoxy compounds. Thermal decomposition of the epoxy resin starts at temperatures above 413 K. To expand this temperature limitation, buried magnets are considered for further investigations. Thus, the maximum rotor temperature is determined by the demagnetization temperature of the magnets.

Due to the increase of rotor complexity with the application of buried magnets, the stress on the rotor is computed by the finite element method. The investigations are performed on a solid rotor, containing cut-outs for the permanent magnets. In order to maximize the rotor radius, the rotor is made of the titanic alloy Ti6Al4V with a tensile yield strength of 1 GPa. Figure 3 depicts the von-Mises stress for different configurations of the rotor with an increasing number of permanent magnet segments. The height of the permanent magnets as well as the inner permanent magnet radius is constant for each configuration, $h_{PM} = 10\,\mathrm{mm}$, $r_{PM} = 11.9\,\mathrm{mm}$. The

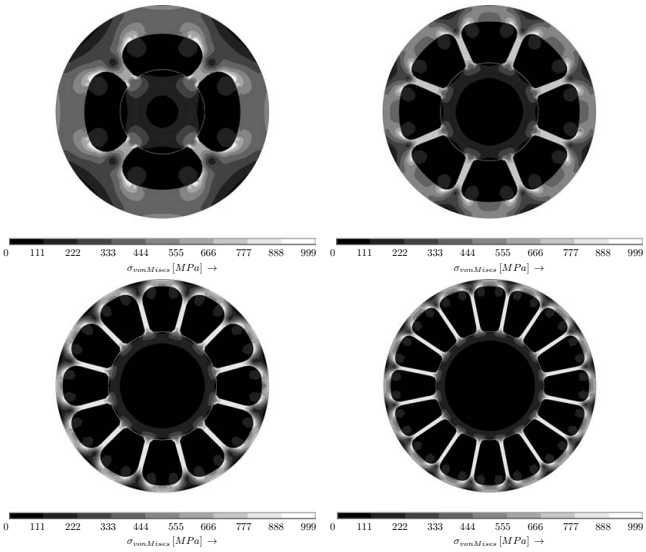

Fig. 3. Comparison of the von-Mises Stress for a different number of permanent magnet segments.

height of the yoke, the radius at the edges of the magnets and the width of the bars between the magnets are adapted in such a way that the maximum von-Mises stress does not exceed the tensile yield strength of 1 GPa. The maximum stress occurs at the edges of the permanent magnet segments. To defuse these hot spots, it is most efficient to bring the permanent magnet segments into a round figure. Increasing the number of permanent magnet segments, the height of the yoke above the magnets as well as the width of the bars between the permanent magnet segments decreases. Thus, the ratio of permanent magnetic material to titanium alloy increases. This implicates an increase of air gap induction whereas the field harmonics decrease as discussed in chapter VI. Hence, a larger number of permanent magnet segments is advantageous regarding to the stress of the rotor and magnetic properties.

IV. Rotor dynamic analysis

The rotor dynamics have to be taken into account during development of high-speed machines. Thus, especially the natural frequencies of the rotor have to be considered, limiting its axial length. To perform rotor dynamic analysis, the whole rotor including the bearings has to be considered. For further investigation, permanent magnetic bearings are considered, as they achieve higher speeds compared to classical bearings. In order to shift the natural frequencies to high values, the rotor bending stiffness has to be maximized, which is achieved by using the cross section of the motor also for the bearings. Thus, the titanium alloy for motor and bearing is manufactured in one piece. The differentiation of the whole rotor in the motor and the bearing part is performed by the direction of magnetizing of the permanent magnet segments. The magnets, which belong to the motor, are magnetized diametrically, whereas the bearing magnets are magnetized alternating in axial direction. Hence, a passive stabilization of radial move-

ment and tilt is performed, whereas the axial stabilization of the rotor has to be achieved by an additional active magnetic bearing, placed at the axial ends of the rotor. Due to the low stiffness of permanent magnetic bearings compared to classical bearings, the volume of one radial bearing is equal to the volume of the active motor part of the rotor as worst case assumption. Thus, the whole volume of the rotor is assumed to be $V_E = 3 \cdot V_R = 354,000\,\mathrm{mm}^3$. The stiffness of one radial bearing is assumed to be $s_B = 250\,{}^{\mathrm{N}}/_{\mathrm{mm}}$. Thus, radial displacement due to weight is less than $\frac{1}{10}\,\mathrm{mm}$.
The investigation of the oscillating behavior is divided into two parts. Firstly, due to the weak stiffness of the magnetic bearings compared to classical bearings, the high-speed rotor is considered as an n-degree-of-freedom (n-DOF) system by the following equation of motion:

$$\mathbf{M}\,\frac{\partial^2 \vec{x}(t)}{\partial t^2} + \mathbf{D}\,\frac{\partial \vec{x}(t)}{\partial t} + \mathbf{S}\,\vec{x}(t) = \vec{d}(t), \tag{13}$$

with the mass matrix:

$$\mathbf{M} = \begin{bmatrix} m & 0 & & \\ 0 & \Theta_a & & \\ & & m & 0 \\ & & 0 & \Theta_a \end{bmatrix}, \tag{14}$$

the damping matrix:

$$\mathbf{D} = \begin{bmatrix} & & 0 & 0 \\ & & 0 & -\omega\Theta_p \\ 0 & 0 & & \\ 0 & +\omega\Theta_p & & \end{bmatrix}, \tag{15}$$

the stiffness matrix:

$$\mathbf{S} = \begin{bmatrix} 2s_B & 0 & & \\ 0 & 2s_B \cdot \frac{l}{2}^2 & & \\ & & 2s_B & 0 \\ & & 0 & 2s_B \cdot \frac{l}{2}^2 \end{bmatrix}, \tag{16}$$

and

$$\vec{x} = [x, \varphi_x, y, \varphi_y]^T.$$

m is the mass of the rotor, $\Theta_{a,p}$ the axial and polar moment of inertia, ω the angular frequency of the rotor, s_B the stiffness of one bearing and l the whole rotor length. The natural frequencies of this system are calculated by:

$$f_{1,3} = \pm\frac{1}{2\pi}\sqrt{\frac{\mathbf{S}_{11}}{m}}, \tag{17}$$

$$f_{2,4} = \frac{1}{2\pi}\left(\frac{\Theta_p}{2\Theta_a}\cdot\omega \pm \sqrt{\left(\frac{\Theta_p}{2\Theta_a}\cdot\omega\right)^2 + \frac{\mathbf{S}_{22}}{\Theta_a}}\right). \tag{18}$$

with:

$$\mathbf{S}_{11} = 2s_B, \tag{19}$$

$$\mathbf{S}_{22} = 2s_B \cdot \frac{l}{2}^2. \tag{20}$$

Due to the gyroscopic effects, the natural frequencies $f_{2,4}$ of nutation and precession depend on the angular frequency ω of the rotor. Special attention has to be paid to achieve different polar Θ_p and axial mass moment of inertia Θ_a. Otherwise, the rotor speed will continuously excite the natural frequency of nutation due to limitations in rotor balance, as depicted in Figure 4. The dependency between the natural frequency of nutation and precession of the bearings and the rotor radius at constant rotor volume V_E is:

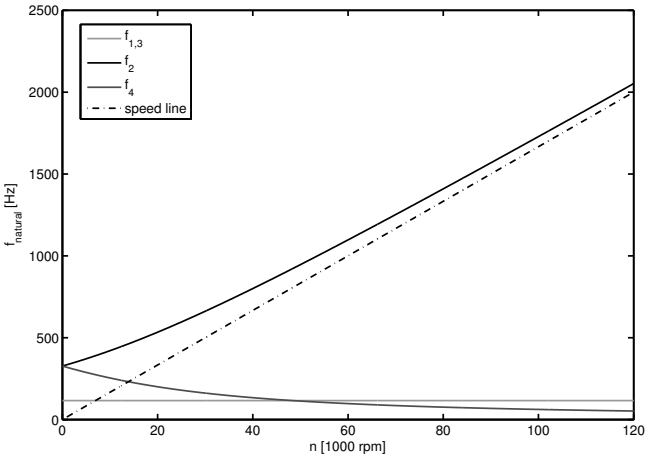

Fig. 4. Campbell diagram for $\Theta_p = \Theta_a$.

$$f_{2,4} \propto \frac{1}{r^3}, \tag{21}$$

whereas $f_{1,3}$ does not depend on the rotor radius.
For the calculation of natural frequencies of the rotor bending mode, the rotor is considered as a continuous system. The application of magnetic bearings with a weak stiffness allows the calculation of the natural frequencies with a negligible shear deformation by a free-free cylinder in standstill for $\frac{2r}{l} < 0.1$ [8]:

$$f_i = \frac{\pi}{8}\left(2\cdot i + 1\right)^2 \cdot \sqrt{\frac{EI}{\rho A_F l^4}}, \tag{22}$$

with the elastic modulus E, the density of rotor material ρ, the cross-sectional area A_F, the planar moment of inertia I and the rotor length l.
The relation between the natural bending frequency at standstill and rotor radius at constant rotor volume V_E is:

$$f_i \propto r^5. \tag{23}$$

Depending on the ratio of inner and outer rotor damping, the operation of high-speed machines can become unstable if the speed line crosses the natural bending frequency line of nutation [4]. To prevent this instability, the first rotor bending frequency of nutation has to be greater than the rotational frequency of the rotor at nominal operation. Due to the weak bearing stiffness, the natural frequencies of the bearings amount only a few tens of hearts and can be passed easily during rotor acceleration.
A detailed investigation of the dynamic behavior of the rotor geometry is performed by finite element analysis. Figure 5 depicts the Campbell diagram of the rotor with 16 permanent

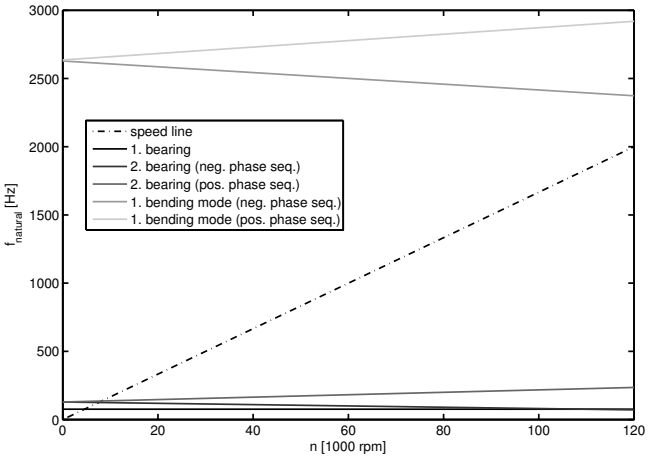

Fig. 5. Campbell diagram for a rotor of a titanium alloy.

magnet segments. The magnets' height is $h_{PM} = 10\,\mathrm{mm}$, the rotor radius amounts to $r = 23.5\,\mathrm{mm}$ and the rotor length, derived from the constant rotor volume V_E, is $l = 204\,\mathrm{mm}$. The magnetic bearings are considered by two perpendicular spring elements with the stiffness $s_B = 250\,\mathrm{N/mm}$. Mechanical rotor properties amounts to $E_{Ti} = 105\,\mathrm{GPa}$, $\nu_{Ti} = 0.2899$, $\rho_{Ti} = 4429\,\mathrm{kg/m^3}$ for titanium alloy and $E_{PM} = 160\,\mathrm{GPa}$, $\nu_{PM} = 0.24$, $\rho_{PM} = 8400\,\mathrm{kg/m^3}$ for the magnets. The uncritical natural frequencies of the bearings are crossed by the speed line, whereas the bending mode of the natural frequency is above the speed line over the whole operation range. Thus, no critical speed is reached, yielding stable operation.

V. Air friction losses

Due to the high circumferential speeds, air friction losses are not negligible in high-speed applications compared to conventional machines, causing an additional heating of the rotor and stator. These losses can be seperated into air gap losses, which occur in the air gap between stator and rotor, as well as losses at the end faces of the rotor. Saari [5] and Nerg et al. [6] investigated these kind of air friction losses in detail. Derived from their results, the dependency of the air friction losses to the outer rotor radius is pointed out.
Furthermore, friction of air particles at the rotor surface induces shear forces to the particles. These shear forces accelerate the air particles in rotary direction. Although losses resulting from the shear forces do not heat the rotor and stator further, an additional breaking torque is applied to the rotor.
Due to the complexity of turbulent air flows, the analytical computations has been adapted to measurement results by experimentally determined friction coefficients.
The nature of the air flow inside the air gap is described by the Reynolds number:

$$Re_\delta = \frac{\rho_c \omega r \delta}{\mu_c}, \tag{24}$$

for the air flow at the end faces:

$$Re_r = \frac{\rho_c \omega r^2}{\mu_c}, \tag{25}$$

and for shear forces due to an axial air flow of an additional cooling gas inside the air gap:

$$Re_a = \frac{\rho_c v_m 2\delta}{\mu_c}, \qquad \text{with} \quad v_m = \frac{\dot{Q}}{A_{air}}. \tag{26}$$

ρ_c is the density and μ_c the dynamic viscosity of the cooling gas. $\dot{Q}$ is the volume flow rate of the cooling gas and A_{air} the cross section of the air gap with the air gap width δ.
The air friction losses inside the air gap are determined by:

$$P_\delta = k_1 C_f \rho_c \pi \omega^3 r^4 l, \tag{27}$$

with the roughness coefficient of the surfaces k_1, the friction coefficient C_f and the rotor length l. The friction coefficient is defined for different Reynold numbers by:

$$C_f = 0.515 \cdot \frac{\left(\frac{\delta}{r}\right)^{0.3}}{Re_\delta^{0.5}} \qquad \left(500 \le Re_\delta \le 10^4\right), \tag{28}$$

$$C_f = 0.0325 \cdot \frac{\left(\frac{\delta}{r}\right)^{0.3}}{Re_\delta^{0.2}} \qquad \left(10^4 < Re_\delta\right). \tag{29}$$

The air friction losses of the end face of the rotor are calculated by:

$$P_{ef} = \frac{1}{2} C_f \rho_c \omega^3 r^5, \tag{30}$$

for the friction coefficients:

$$C_f = \frac{64}{3} \cdot \frac{1}{Re_r} \qquad \left(Re_r < 30\right), \tag{31}$$

$$C_f = \frac{3.87}{Re_r^{0.5}} \qquad \left(30 < Re_r < 3 \cdot 10^5\right), \tag{32}$$

$$C_f = \frac{0.146}{Re_r^{0.2}} \qquad \left(3 \cdot 10^5 < Re_r\right). \tag{33}$$

The losses induced by an additional axial air flow of a cooling medium are determined as:

$$P_{axial} = \frac{2}{3} \pi \rho_c \left((r+\delta)^3 - r^3 \right) v_m u_m \omega, \tag{34}$$

with the mean tangential circumferential speed of the cooling gas at the air gap outlet:

$$u_m = k_2 \cdot \omega r. \tag{35}$$

For smooth rotor and stator surface, k_2 has been experimentally determined to 0.48.
The evaluation of equations 27, 30 and 34 yields a dependency between the rotor radius and the air friction losses at constant rotor volume V_E:

$$P_\delta \propto r^{1\ldots1.6}, \tag{36}$$

$$P_{ef} \propto r^{4\ldots4.6}, \tag{37}$$

$$P_{axial} \propto r^2. \tag{38}$$

Figure 6 depicts the air friction losses depending on the rotor speed and the outer rotor radius. The roughness coefficient is assumed to be $k_1 = 1.0$ for a smooth surface. The density

of the cooling medium air is $\rho_c = 1.225\,\mathrm{kg/m^3}$, the dynamic viscosity of air $\mu_c = 1.8 \cdot 10^{-5}\,\mathrm{kg/ms}$. The air gap width amounts to $\delta = 0.5\,\mathrm{mm}$ at a constant rotor volume of V_E. Thus, in high-speed applications the air friction losses represent several percent of nominal power.

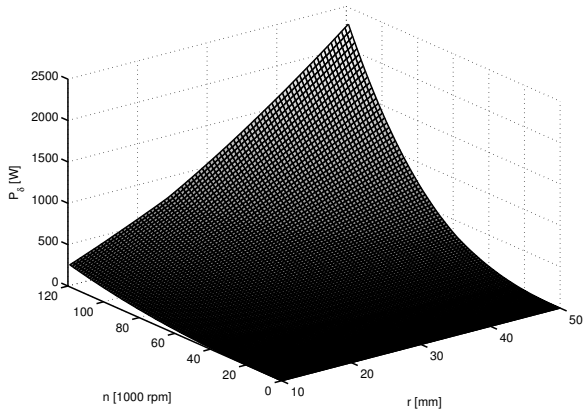

(a) Air gap losses.

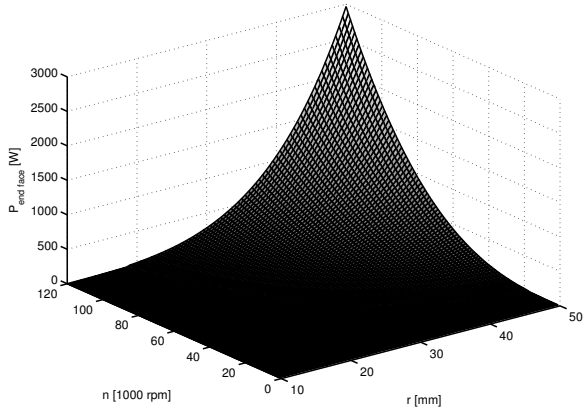

(b) End face losses.

Fig. 6. Air friction losses inside the air gap and at the end face.

VI. Electromagnetic design

Due to the linear dependency between hysteresis losses and the square dependency between eddy current losses and the rotor frequency, especially in high-speed applications the iron losses induced by field harmonics have to be reduced.

In contrast to conventional machines, a reduction of eddy current losses can not be achieved by a lamination of the rotor, which also implies a reduction of bending frequencies and thus in rotor length. Nevertheless, the highest amount of rotor losses is induced by the field harmonics of the stator slots. Due to the distributed air gap winding, this amount of eddy currents omits.

On the other hand, field harmonics of the distributed rotor magnets induce iron losses in the stator back iron. To reduce this kind of losses, a sinusoidal air gap field is essential, which is provided by diametral magnetized surface permanent magnets, shown in Figures 7(a), 7(c) as a function of angular and radial air gap position.

Based on the results of the stress analysis in section III, the permanent magnet segments have to be buried into the rotor as depicted in Figure 7(b). Thus, the permanent magnet ring is splitted into segments, separated by bars of the rotor material. Below, the dependency between the field harmonics and the magnetic return path height t_{PM} above the magnets as well as the width of the separating bars α_{bar} is investigated for ferromagnetic and non-magnetic material.

Due to the saturated magnetic return path t_{PM} above the

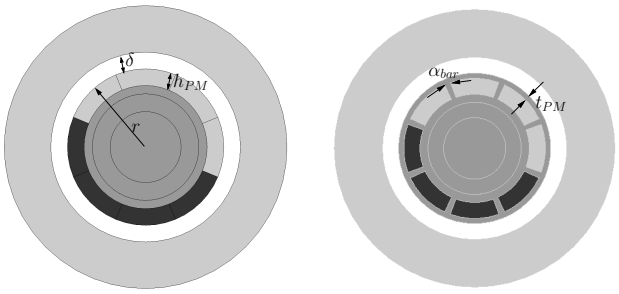

(a) Rotor with surface mounted permanent magnet ring.

(b) Rotor with buried permanent magnets.

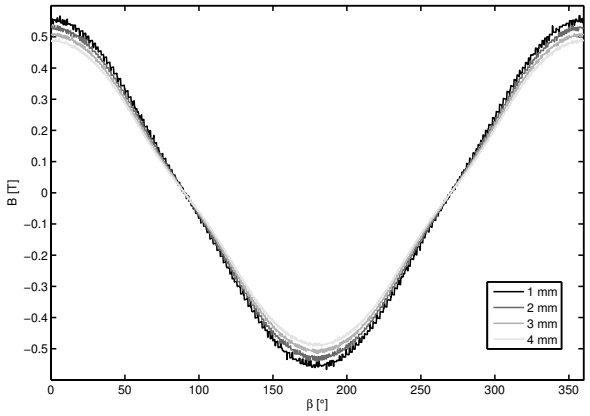

(c) Air gap field of rotor with surface mounted permanent magnets.

Fig. 7. Rotor and air gap field.

permanent magnets in the case of a ferromagnetic rotor material, the 3rd and 5th harmonic of the air gap field increases, as depicted in Figure 8(a) for increasing heights of the magnetic return path. The magnitude of the air gap field is up to 20 % lower compared to the surface mounted permanent magnet ring. The bars between the permanent magnet segments influence the $(n \cdot x \pm 1)$. harmonic with $n \in \mathbb{N}$ and the segmentation number x, shown in Figure 8(b) as function of bar width. The spectral components of the air gap field of a ferromagnetic rotor with $x = 8$ permanent magnet segments, a bar width of $\alpha_{bar} = 5\,^\circ$ and a magnetic return path height of $t_{PM} = 1.6\,\mathrm{mm}$ are depicted in Figure 9(a). To reduce the higher harmonics, inducing additional iron losses in the stator, the magnetic short circuit of the return path between and above the permanent magnet segments is omitted by using a non ferromagnetic rotor material. Figure 9

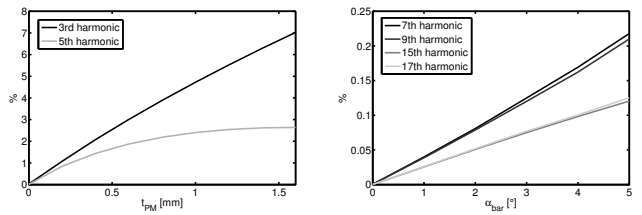

(a) Influence of the deepness of the permanent magnet segments.

(b) Influence of rotor bars using 8 permanent magnet segments.

Fig. 8. Higher harmonics due to segmentation.

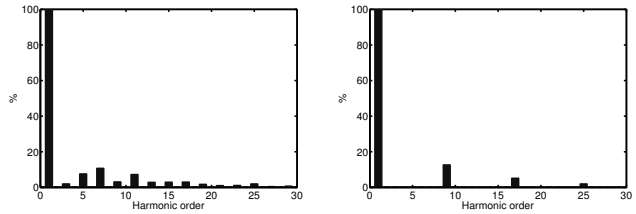

(a) Ferromagnetic alloy.

(b) Titanium alloy.

Fig. 9. Spectral components of the air gap field.

compares the spectral components of these two kinds of rotor material. For the non-magnetic alloy, i.e. the Ti6Al4V alloy, only the $(n \cdot 8 + 1)$. harmonic is significant. Due to the missing magnetic return path in the rotor center, the magnitude of the air gap field is reduced by 12 %. An increase of the permanent magnet height from $h_{PM} = 5\,\mathrm{mm}$ to 10 mm results in an air gap field of the non-magnetic rotor which is even 10 % heigher than the air gap field of the ferromagnetic rotor. Further, the increase of the number of permanent magnet segments x has a positive effect on the magnitude of the air gap field, whereas the amplitude of field harmonics is reduced further. Figure 10 depicts the magnitude of the air gap field for different rotors from Figure 3 at different radial positions in the air gap. Because of the higher effective air gap due to the deeper buried permanent magnet segments as well as the decreasing ratio of permanent magnetic material to titanium alloy, the magnitude of the air gap field decreases by a lower number of permanent magnet segments. Thus, both stress analysis and electromagnetic design prefer an increase of permanent magnet segments' number as well as the adoption of titanium alloy.

VII. Conclusion

This paper describes rotor design criteria for high-speed PMSM. The design is based on a constant rotor volume, which is proportional to the required rated torque. The impact of important rotor properties is investigated first analytically with respect to the rotor radius, as concluded in Table II. Afterwards, the design criteria are applied to an exemplary machine rating 100.000 rpm at 10 kW, applying finite element simulations. Stress analysis have been performed by means of von-Mises criterion. Based on a machine design with magnetic bearings, a rotor concept with buried permanent magnets

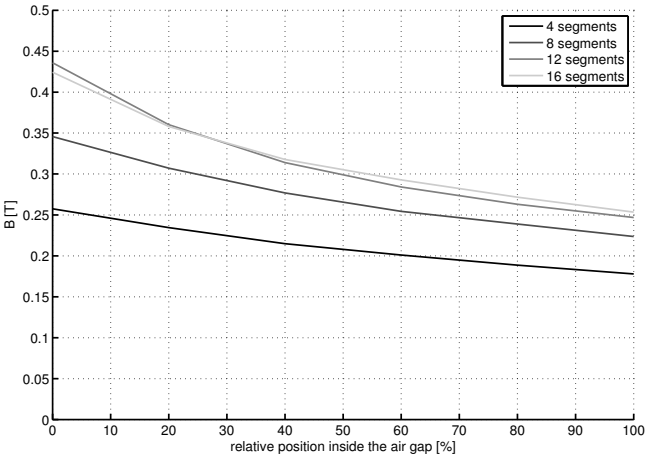

Fig. 10. Influence between the number of permanent magnet segments and the magnitude of the air gap field.

TABLE II
Dependency of important rotor properties with respect to the rotor radius.

Important rotor property	**Dependency on the rotor radius**	**Suggestion to the rotor design**
von-Mises stress	r^2	$r \downarrow$
natural frequency bearing	$\frac{1}{r^3}$	$r \uparrow$
natural frequency bending mode	r^5	$r \uparrow$
air friction losses (air gap)	$r^{1\ldots1.6}$	$r \downarrow$
air friction losses (end face)	$r^{4\ldots4.6}$	$r \downarrow$
air friction losses (axial flow)	r^2	$r \downarrow$

achieves stress criteria best. The rotor is designed for under critical speed range, thus, the speed line does not cross the bending mode of the natural frequency. Air friction losses have been determined in the air gap and at the rotor end faces as well as induced by axial air flow. The air gap field of the rotor is investigated for buried permanent magnet segments. Therefor, a ferromagnetic rotor material and non-magnetic titanium alloy are compared. Due to the non-magnetic return path above and between the permanent magnet segments, the non-magnetic rotor material results in a higher magnitude of the air gap field with decreased spectral components. Increasing the number of permanent magnet segments improves this behavior. In further development, the stator of the high-speed machine as well as the passive radial and active axial magnet bearings have to be investigated and designed. Thereby, special attention must be paid to radial damping of the rotor as well as the computation of eddy current losses and thermal calculations.

References

[1] H. Czichos. *Hütte - Die Grundlagen der Ingenieurwissenschaften.* Springer Verlag, Berlin, Heidelberg, 1989.

[2] G. Müller , B. Ponick. *Theorie elektrischer Maschinen.* WILEY-VCH Verlag, Weinheim, 2009.

[3] G. Müller , K. Vogt, B. Ponick. *Berechnung elektrischer Maschinen.* WILEY-VCH Verlag, Weinheim, 2008.
[4] R. Gasch , R. Nordmann, H. Pfützner. *Rotordynamik.* Springer Verlag, Berlin, Heidelberg, 2006.
[5] J. Saari. *Thermal Analysis of High-speed Induction Machines.* Dissertation, Electrical Engineering Series No. 90, Laboratory of Electromechanics, Helsinki University of Technology, Espoo, 1998.
[6] J. Nerg, M. Rilla and J. Pyrhonen, "Thermal Analysis of Radial-Flux Electrical Machines With a High Power Density", IEEE Trans. on Ind. Electronics, vol. 55, pp. 3543-3554, Oct 2008.
[7] VACUUMSCHMELZE GmbH & Co. KG. *Selten Erd Dauermagnete VACODYM VACOMAX.* www.vacuumschmelze.de. [28.02.2009.]
[8] C. Weißbacher, H. Hübner, R. Sievering, H. Stelzner. *A Small Easy-To-Use Program for Rotor Dynamics.* SIRM 2009 - 8th International Conference on Vibrations in Rotating Machines, Vienna, Austria, February 2009.